EFFECT OF LATERAL VISCOSITY VARIATIONS IN THE CORE-MANTLE BOUNDARY REGION ON PREDICTIONS OF THE LONG-WAVELENGTH GEOID

O. ČADEK[1], L. FLEITOUT[2]

1 Department of Geophysics, Faculty of Mathematics and Physics, Charles University, V Holešovičkách 2, 180 00 Prague, Czech Republic (oc@karel.troja.mff.cuni.cz)

2 Laboratoire de géologie, Ecole normale supérieure, 24, rue Lhomond, 75005 Paris, France (fleitout@geologie.ens.fr)

Received: January 9, 2005; Revised: October 21, 2005; Accepted: November 10, 2005

ABSTRACT

Seismic studies of the lowermost mantle suggest that the core-mantle boundary (CMB) region is strongly laterally heterogeneous over both local and global scales. These heterogeneities are likely to be associated with significant lateral viscosity variations that may influence the shape of the long-wavelength non-hydrostatic geoid. In the present paper we investigate the effect of these lateral viscosity variations on the solution of the inverse problem known as the inferences of viscosity from the geoid. We find that the presence of lateral viscosity variations in the CMB region can significantly improve the percentage fit of the predicted data with observations (from 42 to 70% in case of free-air gravity) while the basic characterisics of the mantle viscosity model, namely the viscosity increase with depth and the rate of layering, remain more or less the same as in the case of the best-fitting radially symmetric viscosity models. Assuming that viscosity is laterally dependent in the CMB region, and radially dependent elsewhere, we determine the large-scale features of the viscosity structure in the lowermost mantle. The viscosity pattern found for the CMB region shows a high density of hotspots above the regions of higher-than-average viscosity. This result suggests an important role for petrological heterogeneities in the lowermost mantle, potentially associated with a post-perovskite phase transition. Another potential interpretation is that the lateral viscosity variations derived for the CMB region correspond in reality to lateral variations in the mechanical conditions at the CMB boundary or to large-scale undulations of a chemically distinct layer at the lowermost mantle.

Key words: core-mantle boundary, D", lateral viscosity variations, geoid, post-perovskite phase transition

1. INTRODUCTION

Boundary regions are generally the most heterogeneous parts of convecting systems. A number of geological and geophysical observations indeed confirm the existence of

significant lateral variations of temperature and chemical composition in the upper 200 km of the mantle. Apart from relatively small-scale heterogeneities, related mainly to plumes, small-scale convection and processes near plate boundaries, we also find heterogeneities over continental scales, associated with lateral changes in lithospheric thickness. These large-scale heterogeneities result in lateral contrasts in viscosity of several orders of magnitude, and may influence the shape of the long-wavelength geoid and dynamic topography at the surface (*Čadek and Fleitout, 2003*).

In comparison with the uppermost part of the mantle, little is known about the bottom boundary layer, denoted as the core-mantle boundary (CMB) region, or D". Our view of its structure is mainly based on seismic research. In spite of certain ambiguities arising from seismic results, there is general agreement with regards to the structural complexity of this region, and a suggestion of the existence of significant heterogeneities over both local and global scales (e.g., *Bijwaard et al., 1998*; *Garnero et al., 2000*; *Tkalcic and Romanowicz, 2002*; *Fisher et al., 2003*; *Thorne and Garnero, 2004*; *Lay et al., 2004*; *Kendall, 2004*). Seismic tomography has recently confirmed that at least some of the hotspots originate in the lowermost mantle (*Montelli et al., 2004*) and has revealed large-scale seismically fast regions in D" that correlate well with the location at the surface of plate convergent zones in the past (*Bijwaard et al., 1998*). If these regions are a graveyard of old slabs, as suggested by some authors (e.g., *Kendall, 2004*), they must be enriched by the chemically distinct material of the former oceanic crust. Such chemical heterogeneities due to segregation processes in the mantle have indeed been predicted in D" by numerical models (*Christensen and Hofmann, 1994*; *Tackley, 2000*). The laterally changing temperature and chemical composition in the CMB region are likely to give rise to lateral viscosity variations over different scales. In this paper, we will attempt to answer the question of whether the large-scale pattern of lateral viscosity variations in D" can be constrained from modeling the gravitational response of the mantle to internal loading.

2. GEOID AND LATERAL VISCOSITY VARIATIONS

The inversion of the long-wavelength non-hydrostatic geoid, known also as the inferences of viscosity from the geoid, has provided important information on mantle viscosity since the mid-eighties (e.g., *Ricard et al., 1984*; *Richards and Hager, 1984*; *Ricard and Bai Wuming, 1991*; *Forte et al., 1994*; *King, 1995*; *Thoraval et al., 1995*; *Kido and Čadek, 1997*; *Steinberger and O'Connell, 1998*; *Čadek and Fleitout, 1999*). Until recently, attention was only paid to determining the radial changes of viscosity. The lateral variations were neglected, partly because of formal reasons (nonlinear coupling in spectral domain), and partly because their effect was assumed to be small in comparison with the radial changes. The last years have seen several efforts to assess the sensitivity of the geoid to lateral viscosity changes (*Richards and Hager, 1989*; *Čadek et al., 1993*; *Zhang and Christensen, 1993*; *King and Hager, 1994*; *Forte and Peltier, 1994*; *Wen and Anderson, 1997*; *Zhong and Davies, 1999*; *Zhong, 2001*; *Čadek and Fleitout, 2003*). Although the answer given in the cited papers is somewhat ambiguous, there are indications that, at least in boundary layers, lateral viscosity variations may play an important role (*Čadek and Fleitout, 2003*). In the top boundary layer, the lateral viscosity variations below the lithosphere determine the mechanical coupling between the

lithospheric plates and the underlying mantle. This may signifficantly influence the prediction of geoid and dynamic topography, especially if the problem of mantle flow is solved with imposed plate velocities. *Čadek and Fleitout (2003)* have demonstrated that the inclusion of lateral viscosity variations in the asthenosphere may improve the fit to data signifficantly: While a model without lateral viscosity variations predicts only 42% of the free-air gravity and 78% of the geoid at degrees 2–8, 67% of the gravity data and more than 90% of the geoid can be explained for the same spectral interval if a simple model with lateral viscosity variations truncated at harmonic degree 4 (in logarithmic scale) is used.

The effect of lateral viscosity variations in the CMB layer on the dynamic geoid has not yet been tested. It follows from the analysis of the geoid kernels obtained for a free-slip core-mantle boundary and radially stratified viscosity models that the loads in the lowermost mantle influence the geoid less than loads in the upper mantle. Moreover, their effect decreases with increasing degree, suggesting only minor effects will arise from the CMB region when predicting the geoid and especially the free-air gravity. On the other hand, large-scale viscosity variations in D" may perturb the flow in the mantle by modulating the mechanical conditions at the core-mantle boundary: The part of D" with a significanly higher-than-average viscosity will effectively behave like a no-slip boundary, despite the fact that free slip is formally prescribed at the CMB.

The effect of large-scale viscosity anomalies in the CMB region may also be amplified by the specific density structure of the lowermost mantle. In contrast to the mid-mantle, where the main density and viscosity variations are presumably associated with narrow plumes and subducting slabs and, thus, show only a small signal at low degrees, the density structure of the bottom 500 km of the mantle displays a very long-wavelength pattern, dominated by degrees 2 and 3 (*Su et al., 1994*). This suggests that the non-linear spectral coupling between flow velocity and the lateral viscosity variations in the lowermost mantle may influence the long-wavelength geoid more than the coupling generated in the rest of the lower mantle.

Motivated by the above considerations, we will test the effect of lateral viscosity variations in the CMB region on the inferences of viscosity from the geoid. We will follow the approach described by *Čadek and Fleitout (2003)*. However, we will only focus our attention on lateral viscosity variations in D" and hence will omit complexities in the viscosity structure elsewhere.

3. FORWARD PROBLEM

To predict the gravitational response of a dynamic mantle, we must solve simultaneously the Laplace-Poisson equation for gravitational potential and the equations governing viscous flow induced by density anomalies in the mantle (*Hager and Clayton, 1989*). The density together with a viscosity structure of the mantle must be speciffied beforehand. The solutions we obtain are gravitational potential, the stress field and the velocity of flow. These quantities can be converted to geoid heights, free-air gravity, dynamic topography and other geophysical observables, and compared with the real data.

The forward problem can be easily solved in the spectral domain, provided viscosity only varies with depth (*Hager and Clayton, 1989*). If a fully 3-D viscosity is considered,

the spectral method must be modified (*Zhang and Christensen, 1993*) or replaced by another, for instance the finite-element method (*Moresi and Gurnis, 1996*; *Zhong and Davies, 1999*). In the present paper, we will use the iterative spectral method proposed by *Colin (1993)* and *Zhang and Christensen (1993)*, and applied in the past to forward and inverse modeling of lateral viscosity variations in the tectosphere (*Čadek and Fleitout, 2003*). This method, which is computationally very fast for the case of a low or intermediate cut-off degree (≤ 100), is especially suitable for the inverse modeling of the long-wavelength geoid, since it allows a large number ($10^6 - 10^7$) of viscosity models to be tested within a reasonable length of time.

For simplicity, we assume that the viscosity of the mantle material is Newtonian (i.e. independent of shear stress) and the material is incompressible. The boundary conditions prescribed at the surface, the 660-km discontinuity and the core-mantle boundary are the same as in *Čadek and Fleitout (2003)*: The observed plate velocities are imposed beneath the lithosphere while traditional free slip and zero radial velocity of flow are prescribed at the core-mantle boundary. The lithosphere is treated as a perfect membrane, with its viscosity going to infinity (*Ribe, 1992*). This membrane is deformed in the radial direction by the stresses acting on its inner boundary in both radial and horizontal directions. The outer boundary of the membrane is assumed to be free-slip. The non-zero radial stress arising at this boundary as a consequnce of the forces acting at the base of the membrane is then interpreted in terms of a dynamic topograhy and used in calculating the dynamic geoid. The flow situation at the upper-lower mantle boundary is characterized by a single parameter, referred to here as the layering coefficient λ, which determines the portion of the layered flow in mantle circulation (for an exact definition, see *Čadek and Fleitout, 1999*). The value of this parameter may range from 0 (whole-mantle flow) to 1 (perfectly layered flow). Although our previous studies have suggested that λ is close to 0.6, we treat it as a free parameter here.

As already mentioned, the solution of the forward problem requires an input model of density anomalies in the mantle to be prescribed. In the present paper, we use a model based on the reconstruction of subducted slabs in the upper mantle and on seismic tomographic information in the lower mantle. Similar density models, combining geological and seismic information, have also been used by other authors (*Hager and Clayton, 1989*; *Ricard et al., 1989*). The reasons why this combined density model is preferred to the entirely tomographic one have been discussed in *Čadek and Fleitout (1999)*. The slab model in the upper mantle is constructed in the same way as in *Ricard et al. (1993)*. We have also tested other upper mantle density models differing from the slab model by *Ricard et al. (1993)* in the density scaling of the slabs. We have found, however, that the result of the inversion for viscosity is only weakly influenced by the specific choice of the density scaling in the upper mantle. In the lower mantle, we use the global tomographic model for S-wave velocity anomalies by *Woodhouse and Trampert (unpublished results)*. We are aware that this tomographic model was developed ten years ago and more recent, high-resolution models are now available (*van der Hilst et al., 1997*; *Bijwaard et al., 1998*; *Montelli et al., 2004*). However, we prefer this model since it has already been used in our previous studies (*Čadek and Fleitout, 1999, 2003*), dealing with the same subject (inferences of viscosity from geoid) but with different parameterizations of viscosity. The use of the same tomographic model in the present study will allow the

results of all three studies to be compared and the effects of lateral viscosity variations to be better understood.

To obtain a density distribution from a model of seismic anomalies, we multiply the seismic velocities by a scaling factor. This factor will be a free parameter and its value will be determined by solving the inverse problem.

4. INVERSION

Our model of the mantle is fully characterized by the following parameters: the layering coefficient, λ, the velocity-to-density scaling factor, s_{LM}, in the lower mantle and the parameters describing the viscosity structure. The lithosphere is assumed to be 100 km thick and, as mentined above, it will be treated as a perfect membrane, with its viscosity going to infinity. Below the lithosphere, the viscosity is parameterized in terms of four layers with interfaces at depths of 100, 200, 660, 2700 and 2900 km. No lateral viscosity variations are considered in the first three layers, with each layer characterized by a single viscosity value, denoted here as η_{asth}, η_{UM} and η_{LM}, respectively. The only layer where lateral viscosity variations are taken into account is in the the core-mantle boundary region (depth interval 2700–2900 km). The viscosity in this layer is parameterized in the logarithmic scale in terms of a spherical harmonic series truncated at degree 4:

$$\log_{10}\eta_{CMB}(\vartheta,\phi)=\sum_{\ell=0}^{4}\sum_{m=-\ell}^{\ell}\eta_{\ell m}Y_{\ell m}(\vartheta,\phi)\,, \tag{1}$$

where Y_{lm} are the complex spherical harmonics, and $\eta_{\ell m}$ are the spherical harmonic coefficients that are to be determined. We assume that the viscosity in the core-mantle boundary region does not vary with radius ($\eta_{\ell m}$ are constant over the depth range 2700–2900 km) and that the viscosity pattern is not necessarily correlated with the distribution of seismic velocity anomalies, i.e. the coefficients $\eta_{\ell m}$ are not a priori constrained by seismic tomographic anomalies. The choice of the relatively low value of the cut-off degree ($\ell_{max}=4$) in Eq.(1) is justified by the increasing difficulties in solving the inverse problem for the case of a large number of model parameters. The total number of free spherical harmonic coefficients is $(\ell_{max}+1)(\ell_{max}+2)/2$, hence 15 if $\ell_{max}=4$. Note that since the boundary condition on the top is formulated in terms of plate velocities, we can determine the absolute values of the viscosity parameters η_{asth}, η_{UM}, η_{LM} and coefficients $\eta_{\ell m}$, and not only the relative ones as is the case if a free-slip upper boundary is considered.

The goal of the inversion is to determine such values of the model parameters that best predict the observed long-wavelength geoid. Since the inversion of the geoid is mainly sensitive to the lowest ($\ell=2;3$) degrees in the geoid spectrum, we will also check the fit to free-air gravity data (*Peltier et al., 1992*). The inverse problem is formulated in the usual way as a least-square minimization of the misfit *S* between the observed and predicted data (*King, 1995*; *Čadek and Fleitout, 1999*):

$$S(\lambda, s_{LM}, \boldsymbol{\eta}) = \int_{\Omega} \left[G^{obs} - G^{pred}(\lambda, s_{LM}, \boldsymbol{\eta}) \right]^2 d\Omega , \tag{2}$$

or, expressed in terms of spherical harmonic coefficients,

$$S(\lambda, s_{LM}, \boldsymbol{\eta}) = \sum_{\ell=2}^{8} \sum_{m=-\ell}^{\ell} \left(G_{\ell m}^{obs} - G_{\ell m}^{pred} \right) \left(G_{\ell m}^{obs} - G_{\ell m}^{pred} \right)^* , \tag{3}$$

where $\boldsymbol{\eta}$ is the vector containing all viscosity parameters,

$$\boldsymbol{\eta} = \{\eta_{asth}, \eta_{UM}, \eta_{LM}, \eta_{\ell m}\} , \ \ell = 0 \ldots 8 , \ m \le \ell , \tag{4}$$

Ω denotes the surface of the Earth, G^{obs} is the observed quantity (geoid height or free-air gravity), G^{pred} is the same quantity predicted for a given set of model parameters, $G_{\ell m}^{obs}$ and $G_{\ell m}^{pred}$ are the spherical harmonic coefficients of the quantities G^{obs} and G^{pred}, respectively, and the asterisk denotes complex conjugation. A relatively low value ($\ell_{max} = 8$) for the cut-off degree in Eq.(3) is chosen, in agreement with the results presented by *Le Stunff and Ricard (1995)*, who have demonstrated that a signifficant part of the geoid signal at degrees $\ell \ge 10$ can be explained by static effects from mass anomalies in the lithosphere.

Since the inverse problem is non-linear, the values of the model parameters that minimize *S* have to be found numerically. To simplify this search, we will first express the predicted geoid as a function of λ, s_{LM} and η_{asth}. Let $\boldsymbol{\eta}_0$ be a vector of the relative values of viscosity,

$$\boldsymbol{\eta}_0 = \boldsymbol{\eta} / \eta_{asth} = \{1, \eta_{UM} / \eta_{asth}, \eta_{LM} / \eta_{asth}, \eta_{\ell m} / \eta_{asth}\} . \tag{5}$$

If the viscosity structure $\boldsymbol{\eta}_0$ is fixed, the prediction of the geoid only depends upon the parameters λ, s_{LM} and η_{asth}. We can write (*Čadek and Fleitout, 1999*):

$$G_{\eta_0}^{pred}(\lambda, s_{LM}, \eta_{asth}) = (1-\lambda) G_{\eta_0}^{WMF}(s_{LM}, \eta_{asth}) + \lambda G_{\eta_0}^{LF}(s_{LM}, \eta_{asth}) , \tag{6}$$

where $G_{\eta_0}^{WMF}(s_{LM}, \eta_{asth})$ is the geoid predicted for viscosity structure $\boldsymbol{\eta}_0$ and parameters s_{LM} and η_{asth}, under assumption of whole mantle flow, while $G_{\eta_0}^{LF}(s_{LM}, \eta_{asth})$ is the geoid obtained for the same parameters but for the layered flow situation. Since $G_{\eta_0}^{WMF}$ and $G_{\eta_0}^{LF}$ depend upon the parameters s_{LM} and η_{asth} linearly, one can easily determine the values of parameters λ, s_{LM} and η_{asth} that minimize the misfit *S* for a chosen viscosity structure $\boldsymbol{\eta}_0$. The inverse problem can therefore be reduced to the search for an optimum vector of the relative viscosity $\boldsymbol{\eta}_0$. To find this vector, we use methods of global search, namely the Monte Carlo method, the genetic algorithm and the method of simulated annealing (*Press et al., 1992*). The agreement between the predicted and observed geoid and/or free-air gravity is characterized by the percentage of the fitted data, or the variance reduction, which is defined as:

$$P = \left(1 - \frac{S}{\left\| G^{obs} \right\|_{L_2}^2} \right) \times 100\% \,, \tag{7}$$

where

$$\left\| G^{obs} \right\|_{L_2}^2 = \int_{\Omega} \left[G^{obs} \right]^2 d\Omega = \sum_{\ell=2}^{8} \sum_{m=-\ell}^{\ell} G_{\ell m}^{obs} \left(G_{\ell m}^{obs} \right)^* . \tag{8}$$

5. RESULTS

The best model found by the global inverse search predicts around 95% of the geoid and 70% of the free air gravity (Fig. 1). We can see that the role of the lateral viscosity variations in the core-mantle boundary region is indeed signifficant: If no lateral viscosity variations are included, only 78% of geoid and 42% of gravity can be explained. The best fitting model is characterized by a strong increase of viscosity with depth ($\eta_{asth} = 4 \times 10^{19}$ Pa s, $\eta_{UM} = 4 \times 10^{20}$ Pa s, and $\eta_{LM} = 8.5 \times 10^{22}$ Pa s), by a layering coefficient $\lambda = 0.6$, and by a velocity-to-density scaling factor $s_{LM} = 0.3$. The predicted pattern of the lateral viscosity variations in the core-mantle boundary region is shown in Fig. 2.

The value of viscosity in the asthenosphere found here is in agreement with the estimate of viscosity based on analysis of the heat flux in oceanic regions (*Dumoulin et al., 1999*). Below the asthenosphere, our inversion prefers a value of 4×10^{20} Pa s, which is compatible with the mean value of viscosity obtained for the upper mantle from inversions of sea-level data (*K. Lambeck, personal communication*). In contrast to postglacial rebound studies, our best-fitting viscosity profile shows rather large (by a factor of 200) increase of viscosity in the lower mantle. Although such an increase of viscosity is larger than usually obtained from inversions of the long-wavelength geoid, it seems compatible with the estimate of viscosity based on stability analysis of plumes (*Steinberger and O'Connell, 1998*).

It should be emphasized, however, that our inversion is nonunique and some parameters cannot be determined with a high degree of accuracy. Whereas the strong increase of viscosity with depth ($\eta_{LM} / \eta_{asth} \approx 10^3$) is a common feature of all well-fitting models, the absolute values of the parameters η_{asth}, η_{UM} and η_{LM} are poorly determined. There is a clear trade-off between the viscosity increase below the asthenosphere (η_{UM} / η_{asth}) and in the lower mantle (η_{LM} / η_{UM}). A realistic prediction of the geoid ($P \geq 90\%$) and free-air gravity ($P \geq 60\%$) can be obtained for a large number of viscosity models, provided $\eta_{LM} / \eta_{UM} \geq 30$ and the lateral viscosity variations in the core-mantle boundary region are included. On the other hand, some other parameters, namely λ and s_{LM}, are well resolved.

This is also valid for the geometry of the lateral viscosity variations in the core-mantle boundary region. We find essentially the same pattern of the viscosity anomalies for all

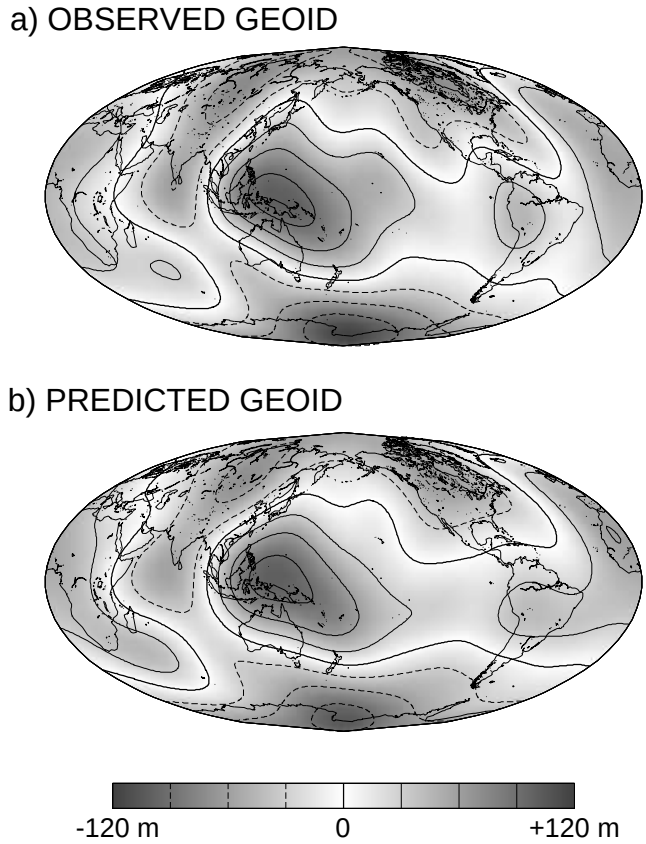

Fig. 1. Comparison between observed and predicted geoids. **(a)** Observed nonhydrostatic geoid ($\ell = 2 \ldots 8$) corrected for the lithospheric effects (*Doin et al., 1996*). **(b)** Geoid predicted in the present study for a viscosity model including laterally variable viscosity in the CMB region. The model predicts 95% of the geoid and 70% of the free-air gravity for degrees 2–8.

models that successfully predict the observed gravitational signal. While the geometry of the lateral viscosity variations is well constrained by the data, their amplitudes may differ for different models. The distribution of the viscosity anomalies in the lowermost mantle is only weakly sensitive to the value of the layering coefficient λ and we have obtained a similar viscosity pattern for the whole-mantle flow model ($\lambda = 0$) as for the best-fitting model with $\lambda = 0.6$.

The lateral viscosity contrasts depicted in Fig. 2 amount to three orders of magnitude, ranging from 5×10^{21} Pa s beneath Central America and the Indian Ocean to 8×10^{24} Pa s beneath the South Atlantic. It should be mentioned, however, that since our computational method is rather time-consuming for large lateral viscosity contrasts, we have not explored a parameter space that includes viscosity contrasts larger than 4 orders of magnitude. The maximum values of viscosity are found in the core-mantle boundary

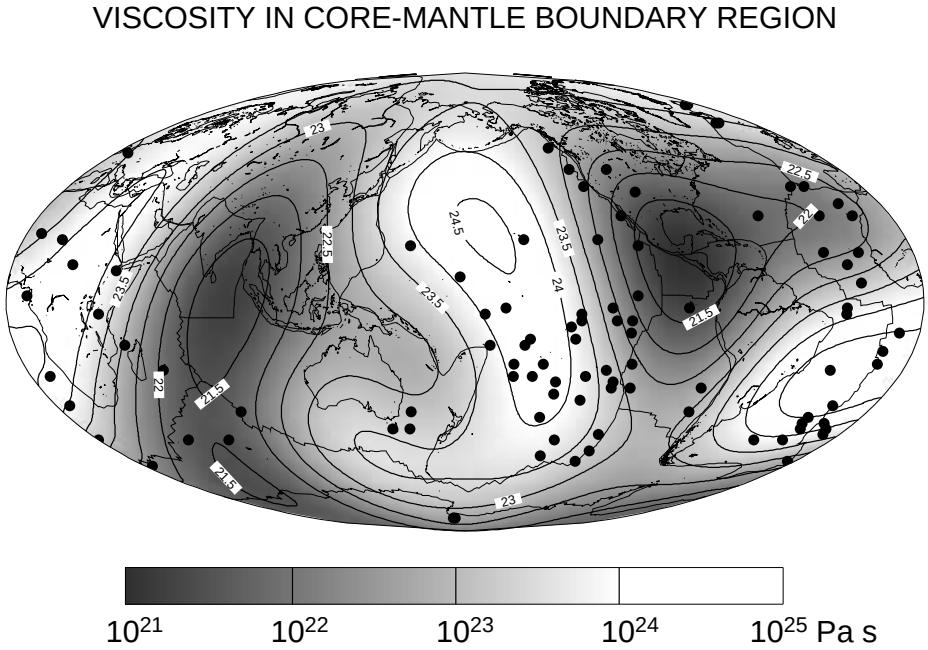

Fig. 2. Lateral viscosity variations in the core-mantle boundary region obtained from the inversion of the geoid. The viscosity (in Pa s) is plotted in logarithmic scale. The dots mark the positions of known hotspots (after *Nataf and Ricard, 1996*).

region beneath the South Atlantic, Africa and the Pacific, thus in areas characterized by a large number of hotspots. From Fig. 2, it is obvious that the relationship between the distribution of the hotspots at the surface and the viscosity anomalies in the CMB region is not random. Strikingly enough, most hotspots are found above the regions of higher-than-average viscosity while only a few hotspots are located above the lowest viscosity regions. A simple statistics (Fig. 3) shows that the surface density of the hotspots may differ by a factor of 5 in dependence on the viscosity of the core-mantle boundary region.

The derived viscosity pattern is weakly anticorrelated with the seismic velocity anomalies at the core-mantle boundary (compare Figs. 2 and 4). In contrast, no statistically signifficant correlation has been found between the viscosity in the CMB region and the location of subduction zones in the past (*Richards and Engebretson, 1992*; *Steinberger, 2000*).

6. OTHER PARAMETERIZATIONS

If both seismic anomalies and lateral viscosity variations were only activated by temperature changes, which is often expected, the amplitudes of viscosity and seismic velocity would have to be in phase. As mentioned above, the viscosity pattern obtained here as a solution of the inverse problem does not satisfy this condition. This result may

indicate the importance of chemical heterogeneity in the CMB region, or it can be interpreted as a consequence of an unsuitably chosen parameterization. To examine the latter possibility, we will test two other parameterizations, both based on the assumption of a purely thermal origin of seismic velocity anomalies and lateral viscosity variations.

The first parameterization is the same as the one described in Section 4, but with the lateral viscosity variations in the CMB region constrained a priori by seismic tomographic data. We assume that

$$\log_{10}\eta_{CMB}(r,\vartheta,\phi) = A + B\delta v(r,\vartheta,\phi), \tag{9}$$

where δv denotes the deviation of seismic velocity from a spherically symmetric reference model, and A and B are positive numbers. The mantle model is then fully characterized by seven parameters, namely λ, s_{LM}, η_{asth}, η_{UM}, η_{LM}, A, and B. Since the number of the model parameters is rather low, we can systematically explore the whole model space and map all models that successfully predict the observed gravitational signal. The best fit to the data is obtained for $B = 0$, that is a model without lateral viscosity variations (cf. *Zhang and Christensen, 1993*). The absence of any lateral viscosity variations in D'' is obviously unrealistic and, moreover, such a model can only explain 78% of geoid and 42% of free-air gravity.

Until now we have only considered the lateral viscosity variations in the lowermost mantle. The next paramaterization is more realistic in that the lateral viscosity variations are included in the whole mantle. As in the previous model, we assume an exponential dependence of viscosity on seismic velocity. In each layer, the viscosity is described by

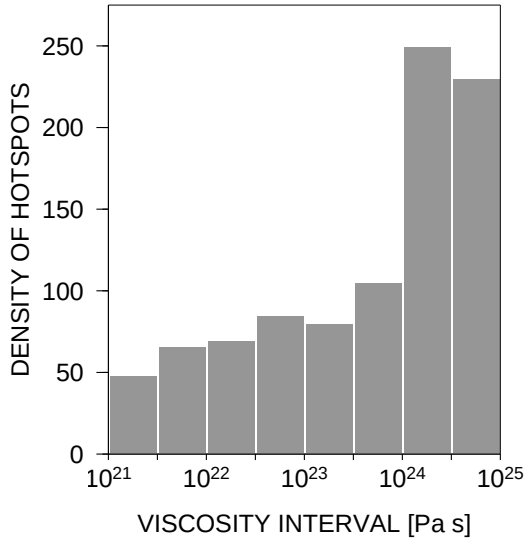

Fig. 3. Density of hotspots as a function of viscosity in the CMB region (Fig. 2). The density is defined as a number of the hotspots located in the region of a given viscosity divided by the relative area of the region (total area of the surface = 1). The viscosity intervals are the same as the isoline intervals in Fig. 2.

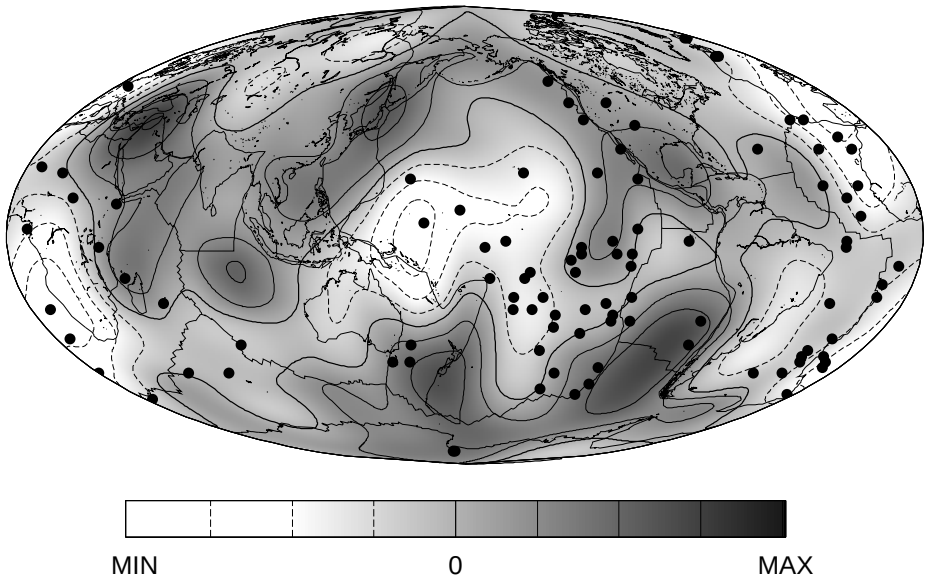

Fig. 4. Lateral variations in shear-wave seismic velocity at a depth of 2850 km plotted for degrees 1–16 (*Woodhouse and Trampert, unpublished results*). The distribution of seismic velocity anomalies is normalized with respect to the maximum value.

two constant parameters, A_i and B_i, such that

$$\log_{10}\eta_i\left(r,\vartheta,\phi\right) = A_i + B_i\delta v\left(r,\vartheta,\phi\right), \tag{10}$$

where index i denotes the number of the layer (i = 1, ..., 4). The interfaces between the layers are located at the same depths as described in Section 4. The optimum values of the parameters A_i and B_i have been determined by combining the technique of the systematic exploration of the model space with a Monte Carlo search. As in the previous case, we have obtained $B_1 = B_2 = B_3 = B4 \sim 0$ (or, more precisely, $B_i\delta v$ □ A_i, i = 1, ..., 4). This means we cannot find a 3-D model of viscosity that predicts the long-wavelength geoid significantly better than a spherically symmetric model. This result indicates that the physical relationship between the lateral viscosity variations and the seismic velocity anomalies may be more complex than assumed in Eq.(10). If mantle material is chemically heterogeneous, the lateral viscosity variations and the seismic velocity anomalies may not be correlated. However, it is possible that the parameterization in Eq.(10) is still oversimplified (e.g., A, B and s_{LM} are likely to depend on depth) or that the results of the inversion are affected by inaccuracies and/or the low resolution in the input tomographic model (e.g., we do not impose stiff and narrow slabs, etc.).

We can conclude that the tested "realistic parameterization" assuming the exponential relationship between viscosity and seismic velocity anomalies does not give satisfactory results. That is why we will hereinafter discuss only the results obtained for the parameterization described in Section 4.

7. DISCUSSION

The results of the inversion described in section 5 clearly prove that the presence of lateral viscosity variations may significantly increase the percentage fit of the predicted data. The improvement of the prediction is especially significant for free-air gravity (from 42% to 70%). The resultant model shows similar features as the model with radially symmetric viscosity, namely a strong increase of viscosity with depth and $\lambda \sim 0.6$ (see *Čadek and Fleitout, 1999*), but because of the lateral viscosity variations in the lowermost mantle, it gives a more realistic prediction of the gravitational data.

The results of the studies dealing with the effects of lateral viscosity variations on the geoid have so far been somewhat ambiguous. While some authors report that these effects are significant, other studies indicate that the lateral viscosity variations have little influence on the long-wavelength geoid in comparison with the radial changes in viscosity. The results presented here and in the paper by *Čadek and Fleitout (2003)* suggest that the large-scale anomalies in the boundary layers do play an important role. Their effect can intuitively be understood if we realize that the lateral increase of viscosity acts in the same way as a no-slip boundary condition (*Ravine and Phipps Morgan, 1993*). Whereas the low-viscosity regions effectively behave as a free-slip boundary, we obtain an additional tangent force in regions of higher-than-average viscosity. This force then influences mantle flow and, consequently, the geoid.

The weakly negative correlation between the derived viscosity field and the seismic pattern in the CMB region suggests the importantance of lateral petrological changes in the lowermost mantle. If only the thermal effects were important, then the two fields would be positively correlated. Another possible interpretation has already been suggested in the previous paragraph: since the lateral viscosity variations in the layer above the CMB influence the flow in the mantle in a similar way as a laterally variable boundary condition, we can interpret them in terms of laterally changeable mechanical conditions at the CMB. The regions of very high viscosity are basically stagnant and, thus, can be replaced by a no-slip boundary condition. In contrast, the material in regions of lower-than-average viscosity can flow more freely, corresponding to a free-slip boundary condition.

This concept can also help us to reconcile the fact that most hotspots are located over regions of higher-than-average viscosity. These regions, interpreted now as parts of the CMB with a no-slip boundary condition, can be identified with a thin layer of a dense material of crustal origin lying on top of the core (*Hofmann and White, 1982*; *Christensen and Hoffman, 1994*; *Coltice and Ricard, 1999*). As shown by *Tackley (2000)*, such a material cannot move rapidly in the lateral direction, which is consistent with the no-slip boundary condition. Some geochemical data indicate that this layer may indeed be the source of plumes (*Hofmann and White, 1982*) and consequently of hotspot volcanism (*Morgan, 1971*). Since the plumes originate in a laterally stagnant environment, their positions change little over time, which is in agreement with the observed hotspot stability.

The material lying at the CMB can hardly be detected by global seismic tomography and its gravitational effect is negligible because it is isostaticly compensated. In contrast, the plumes in the mantle above the CMB region are imaged by seismic tomography as

large seismically slow regions (*Čadek et al., 1995*). Since buoyant and actively upwelling lower-mantle structures below the Pacific and Africa are necessary for a successful prediction of the geoid, these regions must be on average less dense than the surrounding mantle (see also *Panning and Rabinowicz, 2004*). It is therefore natural to assume that the large-scale negative seismic anomalies in the lower mantle are mainly of a thermal origin, and that chemical heterogeneity is only important in the close vicinity of the CMB.

It is also possible that the lateral viscosity variations obtained here as a solution of the inverse problem are associated with a post-perovskite phase transition, recently suggested by mineral physicists (*Murakami et al., 2004*). The results by *Tsuchyia et al. (2004)* and *Hirose and Fujita (2005)* indicate a large positive Clapeyron slope, which would mean that the phase boundary is depressed or even absent in hotter regions. If the post-perovskite phase is less viscous than perovskite, than this would lead to higher viscosities in hotter regions, contrary to what is usually expected.

Our results may also reflect the existence of a chemically distinct layer in the lowermost mantle (*B. Steinberger, personal communication*). Such a layer would be piled up beneath large-scale upwellings, with the elevated regions being a source of plumes as it has been suggested by *Davaille et al. (2002)* and *Jellinek and Manga (2002)*. Piling up such a layer beneath upwellings would cause restoring forces trying to flatten the layer out again. These forces would reduce the horizontal flow towards the upwellings in the layer above, in a similar way as if a no-slip boundary condition were prescribed on the top of this layer. If a chemically distinct layer is not included in the model, but lateral viscosity variations are, the presence of this layer is manifested by the distribution of lateral viscosity variations that is equivalent to a no-slip boundary condition below large-scale upwellings.

8. CONCLUSIONS

Lateral viscosity variations in the core-mantle boundary region can significantly influence predictions of the long-wavelength gravitational data. The best fit to the data has been obtained for viscosity variations ranging from 5×10^{21} to 8×10^{24} Pa s. The derived viscosity pattern correlates with neither the distribution of seismic velocity anomalies in the lowermost mantle, nor with the positions of subduction zones in the last 180 Myr. In contrast, the lateral viscosity variations in the CMB region are clearly related to the distribution of hotspots at the surface (i.e. high density of hotspots above the regions of higher-than-average viscosity). These results therefore suggest an important role for chemical heterogeneity in the lowermost mantle. Another possible explanation is that the lateral viscosity variations obtained here for the CMB region correspond in reality to lateral variations of mechanical conditions at the core-mantle boundary. This interpretation is in agreement with some geochemical concepts (*Hofmann and White, 1982*; *Coltice and Ricard, 1999*) and naturally explains the high occurrance of hotspots above the apparent viscosity maxima in the CMB region. It is also possible that the viscosity pattern obtained in the lowermost mantle reflects undulations of a chemically distinct layer (*Davaille et al., 2002*; *Jellinek and Manga, 2002*) or a post-perovskite phase transition (*Murakami et al., 2004*).

The viscosity structure of the CMB region presented in this paper may be affected by a number of simplifications that are justified by the adopted modelization method and by our limited knowledge of the physical parameters of the mantle. We neglect (i) spatial variability in the velocity-to-density scaling factor in the lower mantle, (ii) lateral viscosity variations in the mantle above the CMB layer, and (iii) continuous changes of viscosity with depth inside the layers. Moreover, we significantly simplify (iv) the density structure in the mantle as well as (v) the flow situation at the upper/lower-mantle boundary (the resistive force acting in the transition zone is parameterized by a single parameter).

Independently of these simplifications, our study has demonstrated that lateral viscosity variations in the boundary layer are important when modeling the long-wavelength gravitational signal and their inclusion can lead to a significantly better prediction of the data in comparison with radially symmetric models. The inverse modeling of the lateral viscosity variations in the lowermost mantle is strongly complicated by the lack of additional observational constraints. It is obvious that without such constraints, our viscosity models necessarily remain speculative.

Acknowledgements: We thank J. Trampert for providing the coefficients of his tomographic model, B. Steinberger for valuable comments and suggestions, and K. Fleming for reading the manuscript. This work has been supported by the Czech national grant GACR 205/02/1306.

References

Bijwaard H., Spakman W. and Engdahl E.R., 1998. Closing the gap between regional and global travel time tomography. *J. Geophys. Res.*, **103**, 30,055–30,078.

Čadek O. and Fleitout L., 1999. A geoid model with imposed plate velocities and partial layering. *J. Geophys. Res.*, **104**, 29,055–29,075.

Čadek O. and Fleitout L., 2003. Effect of lateral viscosity variations in the top 300 km on the geoid and dynamic topography. *Geophys. J. Int.*, **152**, 566–580.

Čadek O., Kývalová H. and Yuen D.A., 1995. Geodynamical implications from the correlation of surface geology and seismic tomographic structure. *Earth Planet. Sci. Lett.*, **136**, 615–627.

Čadek O., Ricard Y., Martinec Z. and Matyska C., 1993. Comparison between Newtonian and non-Newtonian flow driven by internal loads. *Geophys. J. Inter.*, **112**, 103–114.

Colin P., 1993. *Géoid global, topographie associée et structure de la convection dans le manteau terrestre: Modélisation et observation*. Ph.D. Thesis, Ecole normale supérieure, Paris, France.

Coltice N. and Ricard Y., 1999. Geochemical observations and one layered mantle convection. *Earth Planet. Sci. Lett.*, **174**, 125–137.

Christensen U.R. and Hofmann A.W., 1994. Segregation of subducted oceanic crust in the convecting mantle. *J. Geophys. Res.*, **99**, 19,867–19,884.

Davaille A., Girard F. and Le Bars M., 2002. How to anchor hotspots in a convecting mantle? *Earth Planet. Sci. Lett.*, **203**, 621–634.

Doin M.-P., Fleitout L. and McKenzie D., 1996. Geoid anomalies and the structure of continental and oceanic lithospheres. *J. Geophys. Res.*, **101**, 16,119–16,135.

Dumoulin C., Doin M.-P. and Fleitout L., 1999. Heat transport in stagnant lid convection with temperature- and pressure-dependent Newtonian or non-Newtonian rheology. *J. Geophys. Res.*, **104**, 12,759–12,777.

Forte A.M. and Peltier W.R., 1994. The kinematics and dynamics of poloidal-toroidal coupling in mantle flow: The importance of surface plates and lateral viscosity variations. *Advances in Geophysics*, **36**, 1–119.

Forte A.M., Woodward R.L. and Dziewonski A.M., 1994. Joint inversions of seismic and geodynamical data for models of three-dimensional mantle heterogeneity. *J. Geophys. Res.*, **99**, 21,857–21,877.

Fisher J.L., Wysession M.E. and Fischer K.M., 2003. Small-scale lateral variations in D" attenuation and velocity structure. *Geophys. Res. Lett.*, **30**, Art. No. 1435.

Garnero J.E., Revenaugh J., Williams Q., Lay T. and Kellogg L.H., 2000. Ultralow velocity zone at the core-mantle boundary. In: M. Gurnis, M.E. Wysession, E. Knittle and B.A. Buffett (Eds.), *The Core-Mantle Boundary Region*, *Geophysics Series*, **28**, AGU, Washington, D.C., 319–334.

Hager B.H. and Clayton, R.W., 1989. Constraints on the structure of mantle convection using seismic observations, flow models, and the geoid. In: W.R. Peltier (Ed.), *Mantle Convection: Plate Tectonics and Global Dynamics*, Gordon and Breach, Newark, N.J., 657–763.

Hirose K. and Fujita Y., 2005. Clapeyron slope of the post-perovskite phase transition in $CaIrO_3$. *Geophys. Res. Lett.*, **32**, L13313, doi:10.1029/2005GL023219.

Hofmann A.W. and White W.M., 1982. Mantle plumes from ancient oceanic crust. *Earth Planet. Sci. Lett.*, **57**, 421–436.

Jellinek A.M. and Manga M., 2002. The inuence of a chemical boundary layer on the fixity and lifetime of mantle plumes. *Nature*, **418**, 760–763.

Kendall M., 2004. Tectonics of the lower mantle. *Astron. Geophys.*, **45**, 30–34.

Kido M. and Čadek O., 1997. Inferences of viscosity from oceanic geoid: Indication of a low viscosity zone below the 660-km discontinuity. *Earth Planet. Sci. Lett.*, **151**, 125–138.

King S.D., 1995. Radial models of mantle viscosity: Results from a genetic algorithm. *Geophys. J. Int.*, **122**, 725–734.

King S.D. and Hager B.H., 1994. Subducted slabs and the geoid: 1) numerical calculations with temperature-dependent viscosity. *J. Geophys. Res.*, **99**, 19,843–19,852.

Lay T., Garnero E.J. and Russell S.A., 2004. Lateral variations of the D" discontinuity beneath the Cocos Plate. *Geophys. Res. Lett.*, **31**, L15612.

Le Stunff Y. and Ricard Y., 1995. Topography and geoid due to lithospheric mass anomalies. *Geophys. J. Int.*, **122**, 982–990.

Montelli R., Nolet G., Dahlen F.A., Masters G., Engdahl E.R. and Hung S.H., 2004. Finite-frequency tomography reveals a variety of plumes in the mantle. *Science*, **303**, 338–343.

Moresi L. and Gurnis M., 1996. Constraints on the lateral strength of slabs from threedimensional dynamic flow models. *Earth Planet. Sci. Lett.*, **138**, 15–28.

Morgan W.J., 1971. Convection plumes in the lower mantle. *Nature*, **230**, 42–43.

Murakami M., Hirose K., Kawamura K., Sata N. and Ohishi Y., 2004. Post-perovskite phase transition in $MgSiO_3$. *Science*, **304**, 855–858.

Nataf H.C. and Ricard Y., 1996. 3SMAC: An a priori tomographic model of the upper mantle based on geophysical modeling. *Phys. Earth Planet. Inter.*, **95**, 101–122.

Panning M. and Romanowicz B., 2004. Inferences on ow at the base of Earth's mantle based on seismic anisotropy. *Science*, **303**, 351–353.

Peltier W.R., Forte A.M., Mitrovica J.X. and Dziewonski A.M., 1992. Earth's gravitational field: Seismic tomography resolves the enigma of the Laurentian anomaly. *Geophys. Res. Lett.*, **19**, 1555–1558.

Press V.H., Teukolsky S.A., Wetterling W.T. and Flannery B.P., 1992. *Numerical Recipes in Fortran. The Art of Scientific Computing*. Cambridge University Press, Cambridge.

Ravine M.A. and Phipps Morgan J., 1993. Geoid effects of lateral viscosity variations near the top of the mantle: a 2D model. *Earth Planet. Sci. Lett.*, **119**, 617–625.

Ribe N.M., 1992. The dynamics of thin shells with variable viscosity and the origin of toroidal flow in the mantle. *Geophys. J. Int.*, **110**, 537–552.

Ricard Y. and Bai W., 1991. Inferring viscosity and the 3-D density structure of the mantle from geoid, topography and plate velocities. *Geophys. J. Int.*, **105**, 561–572.

Ricard Y., Fleitout L. and Froidevaux C., 1984. Geoid heights and lithospheric stresses for a dynamic Earth. *Ann. Geophys.*, **2**, 267–286.

Ricard Y., Richards M.A., Lithgow-Bertelloni C. and Le Stunff Y., 1993. A geodynamic nodel of mass heterogeneity. *J. Geophys. Res.*, **98**, 21,895–21,909.

Ricard Y., Vigny C. and Froidevaux C., 1989. Mantle heterogeneities, geoid, and plate motion - a Monte Carlo inversion. *J. Geophys. Res.*, **94**, 13,739–13,754.

Richards M.A. and Engebretson D.C., 1992. Large-scale mantle convection and the history of subduction. *Nature*, **355**, 437–440.

Richards M.A. and Hager B.H., 1984. Geoid anomalies in a dynamic Earth. *J. Geophys. Res.*, **89**, 5987–6002.

Richards M.A. and Hager B.H., 1989. Effects of lateral viscosity variations on long wavelength geoid anomalies and topography. *J. Geophys. Res.*, **94**, 10,299–10,313.

Steinberger B. and O'Connell R.J., 1998. Advection of plumes in mantle flow: Implication for hotspot motion, mantle viscosity and plume distribution. *Geophys. J. Int.*, **132**, 412–434.

Steinberger B., 2000. Slabs in the lower mantle - results of dynamic modelling compared with tomographic images and the geoid. *Phys. Earth Planet. Inter.*, **118**, 241–257.

Su W.J., Woodward R.L. and Dziewonski A.M., 1994. Degree-12 model of shear velocity heterogeneity in the mantle. *J. Geophys. Res.*, **99**, 6945–6980.

Tackley P., 2000. Three-dimensional simulations of mantle convection with a thermochemical basal boundary layer: D"?. In: M. Gurnis, M.E. Wysession, E. Knittle and B.A. Buffett (Eds.), *The Core-Mantle Boundary Region, Geophysics Series*, **28**, AGU, Washington, D.C., 231–253.

Thoraval C., Machetel P. and Cazanave A., 1995. Locally layered convection inferred from dynamic models of the Earth's mantle. *Nature*, **375**, 777–780.

Thorne M.S. and Garnero E.J., 2004. Inferences on ultralow-velocity zone structure from a global analysis of SPdKS waves. *J. Geophys. Res.*, **109**, B08301.

Tkalcic H. and Romanowicz B., 2002. Short scale heterogeneity in the lowermost mantle: insights from PcP-P and ScS-S data. *Earth Planet. Sci. Lett.*, **201**, 57–68.

Tsuchiya T., Tsuchyia J., Umemoto K. and Wentzcovitch R.M., 2004. Phase transition in $MgSiO_3$-perovskite in the earth's lower mantle. *Earth Planet. Sci. Lett.*, **224**, 241–248.

van der Hilst R.D., Widiyantoro S. and Engdahl E.R., 1997. Evidence for deep mantle circulation from global tomography. *Nature*, **386**, 578–584.

Wen L. and Anderson D.L., 1997. Present-day plate motion constraint on mantle rheology and convection. *J. Geophys. Res.*, **102**, 24,639–24,653.

Zhang S. and Christensen U.R., 1993. Some effects of lateral viscosity variations on geoid and surface velocities induced by density anomalies in the mantle. *Geophys. J. Int.*, **114**, 531–547.

Zhong S., 2001. Role of ocean-continent contrast and continental keels on plate motion, net rotation of lithosphere, and the geoid. *J. Geophys. Res.*, **106**, 703–712.

Zhong S. and Davies G.F., 1999. Effects of plate and slab viscosities on the geoid. *Earth Planet Sci. Lett.*, **170**, 487–496.